Supporting Information

MOF-on-MOF NiFe-BDC@ZIF-67 Heterostructure Nanoarrays for Chloride-Suppressed Oxygen Evolution in Alkaline Seawater

Yanhui Lu [a], Muhammad Murad [a], Donglei Guo [b, *], Chengang Pei [a], Xu Yu [a, *]

[a] Jiangsu Provincial Key Laboratory of Green & Functional Materials and Environmental Chemistry, School of Chemistry and Materials, Yangzhou University, Yangzhou, Jiangsu 225002, P. R. China

[b] Key Laboratory of Function-Oriented Porous Materials, College of Chemistry and Chemical Engineering, Luoyang Normal University, Luoyang 471934, P. R. China;

Corresponding author:
Email:yxypz15@yzu.edu.cn (X. Yu); *guodonglei@lynu.edu.cn* (D. Guo)

S1. Characterization

Powder X-ray diffraction (XRD) patterns were recorded on a Bruker D8 Advance powder X-ray diffractometer using a Cu Kα (λ = 1.5405 Å) radiation source operating at 40 kV and 40 mA with the scanning rate of 5°/min. Raman spectra were recorded using a Laser confocal Raman spectrometer (Renishaw inVia, Britain) with a laser excitation of 532 nm. Fourier transform infrared spectrometer (FTIR, 670-IR, America) was employed to determine the presence of the organic ligand; the wavelength was selected from 4000 to 400 cm^{-1}. The morphology and microstructure of the product were analyzed by scanning electron microscopy (FESEM, Hitachi, S-4800 II, Japan) and transmission electron microscopy (TEM, FEI, Tecnai G2 F30 S-TWIN, America). All X-ray photoelectron spectroscopy (XPS) measurements were carried out on Kratos XSAM-800 spectrometers with an Al Kα radiation source.

S2. Experimental section

Synthesis of the NiFe-BDC

1 mmol of benzenedicarboxylic acid (BDC) was ultrasonically dissolved in 10 mL of N, N-dimethylformamide (DMF). Next, 30 mL of ethanol was poured into the above solution to form a homogeneous solution. After that, 1 mmol of $FeCl_3 \cdot 6H_2O$ was dissolved in the solution. Finally, the obtained yellow solution was transferred into a Teflon-lined stainless-steel autoclave, and a piece of NF (3*5 cm^2) was vertically immersed. The autoclave was sealed and heated at 140 °C for 12 h and then cooled naturally to room temperature. The resulting sample was washed thoroughly with ethanol and deionized water three times each and dried at 60 °C under vacuum for 6 h to obtain NiFe-BDC.

Synthesis of NiFe-BDC@ZIF-67

The as-prepared NiFe-BDC was vertically immersed in the beaker containing 40 mL of methanol with $Co(NO_3)_2 \cdot 6H_2O$ (2 mmol) and 2-methylimidazole (2-mlm, 16 mmol). The mixture was prepared by vigorously stirring for 10 min and aged at room temperature for 6 h. During this period, the Co^{2+} ions and 2-mIm ligands in the solution slowly diffused to the surface of the NiFe-BDC framework, where they coordinated, nucleated, and epitaxially grew to form a uniform ZIF-67 shell. Finally, the product was ultrasonically cleaned with methanol and ethanol several times to remove loosely adsorbed particles and dried at 60 °C under vacuum, yielding the final NiFe-BDC@ZIF-67 catalyst. The mass loading of NiFe-BDC@ZIF-67 on the NF substrate is about 1.2 $mg \cdot cm^{-2}$.

S3. Electrochemical measurements

The electrochemical measurements were performed in a 1.0 M KOH electrolyte at room temperature using an electrochemical workstation (CHI660E) with a three-electrode system. The 1 M KOH + seawater electrolyte was prepared by first filtering the natural seawater through a 0.22 μm membrane to remove suspended particles. No additional purification or desalination steps were performed during this process to preserve the original ionic composition. The filtered seawater was then used to prepare the alkaline electrolyte with a concentration of 1 M KOH. The glass carbon electrode (GC, diameter 3 nm, 0.07 cm^2) was used as the supporting working electrode to measure HER performance. Graphite rod and saturated calomel electrode (SCE) were used as the counter and reference electrodes, respectively. The catalytic ink is prepared as below. The resulting electrocatalyst was used as a working electrode with a size of 1*1 cm^2. All potentials were referenced to a reversible hydrogen electrode (RHE); the formula is as follows: E(RHE) = E(SCE) + 0.059*pH + 0.242V.

The polarization curves were measured by cyclic voltammetry (CV) at a scan rate of 5 mV s^{-1} with 90% IR correction. The ohmic resistance with IR correction was obtained using electrochemical impedance spectroscopy in the frequency range of 1000 kHz~10 mHz with an amplitude of 5 mV. The durability test was carried out for 1000 cyclic voltammetry (CV) cycles at a scan rate of 150 mV s^{-1}, and a linear sweep was measured at a scan rate of 5 mV s^{-1} after 1000 cycles. The electrochemically active surface area (ECSA) was estimated from the electrochemical double-layer capacitance (C_{dl}) by measuring CV curves at different scan rates in a non-Faradaic region. A chronoamperometry (CA) test was carried out at the potential of 1.50, 1.55, 1.62 and 1.80 V vs. RHE for 100 h. After the CA test, the SEM, TEM, XRD and XPS of the active catalyst were carried out.

The apparent electrochemical activation energy (E_a) for HER can be determined using the Arrhenius plots, according to the equation:

$$\frac{\partial log(j_0)}{\partial(1/T)} = -\frac{E_a}{2.303R}$$

Where j_0 is the exchange current density, R is the universal gas constant (8.314 J mol^{-1} K^{-1}), and T is the absolute temperature.

Faradaic efficiency was measured at 200 mA cm^{-2} for 1 h. The amount of O_2 generated was determined by monitoring the pressure changes in a sealed electrolytic

cell using a manometer (CEM DT-8890), and the moles of O_2 produced were calculated based on the following equation.

$$Faradaic\ yield = \frac{V_{Exp}}{V_{Theor}} = \frac{V_{Exp}}{\frac{1}{4} * \frac{Q}{F} * V_m}$$

Where the V_{Exp} and V_{Theor} are the experimental and theoretical volumes of the generated O_2 gas during the catalytic process, Q is the charge passed through the electrode, F is the Faraday constant (96485 C mol^{-1}), and V_m is the molar volume of gas (24.5 L mol^{-1}, 298 K, 101 KPa).

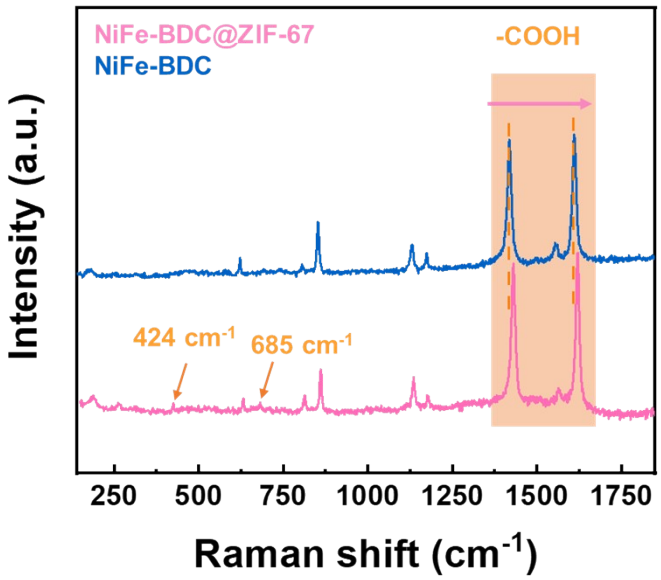

Figure S1 Raman spectra of NiFe-BDC@ZIF-67 and NiFe-BDC.

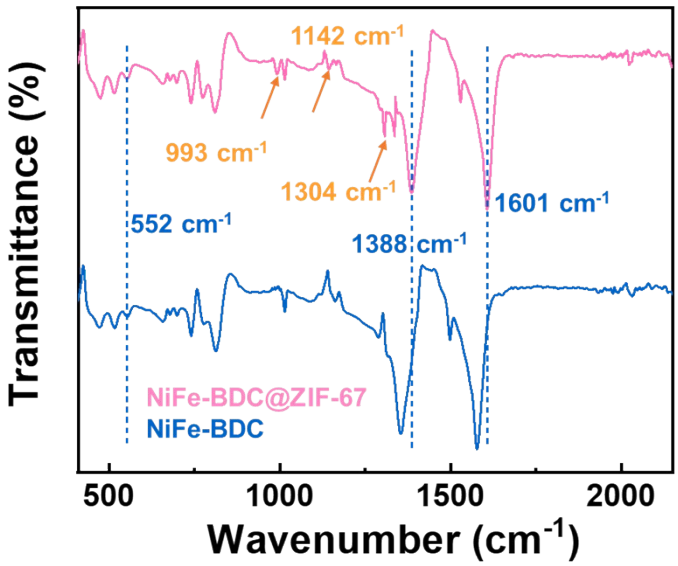

Figure S2 FTIR spectra of NiFe-BDC@ZIF-67 and NiFe-BDC.

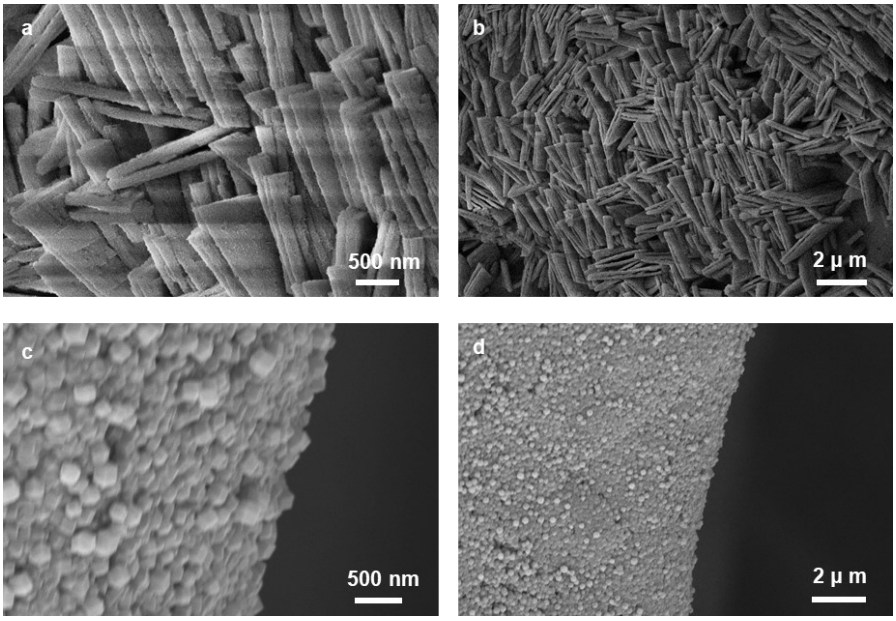

Figure S3 SEM of the (a, b) NiFe-BDC and (c, d) ZIF-67.

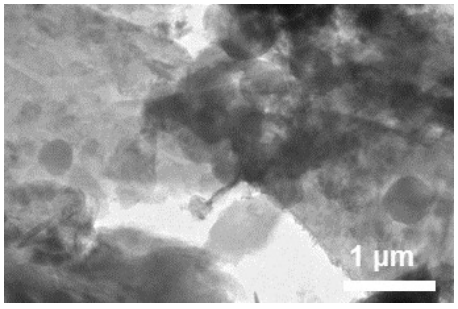

Figure S4 TEM of NiFe-BDC@ZIF-67.

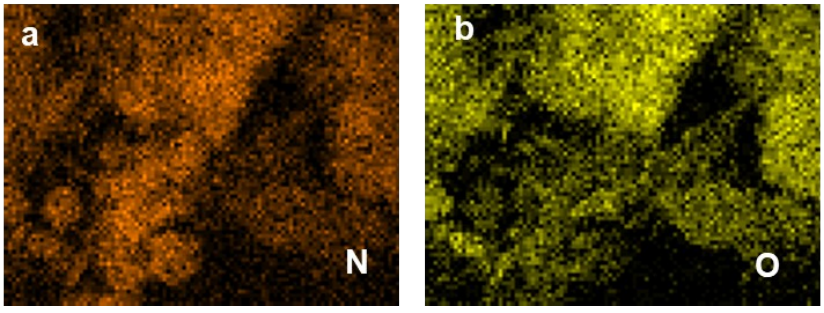

Figure S5 elemental mappings of NiFe-BDC@ZIF-67.

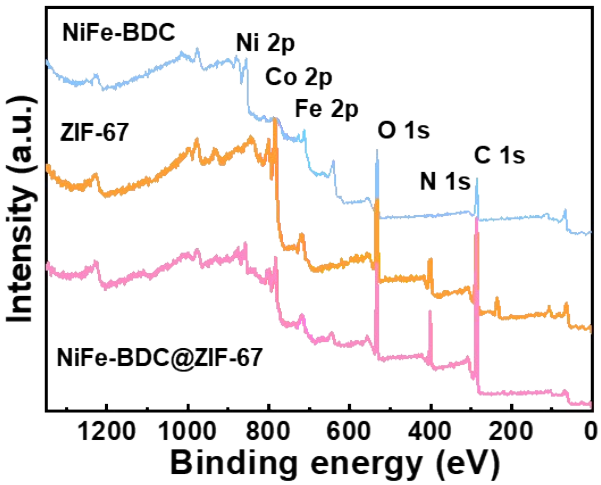

Figure S6 XPS full survey spectra of different samples.

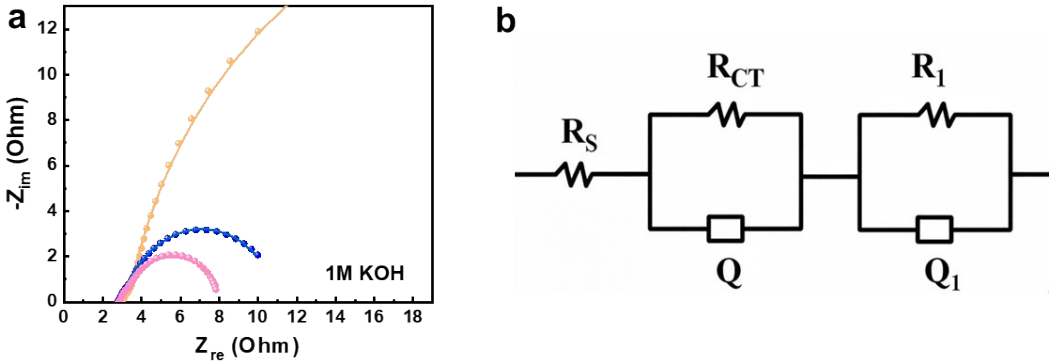

Figure S7 (a) EIS of different samples, (b) Randles equivalent circuit.

The EIS data was fitted following the equivalent circuit diagram to obtain the corresponding resistance values including the equivalent resistance of the system (R_s), charge transfer resistance (R_{ct}) and adsorption resistance (R_1), the non-ideal double-layer capacitance at the electrode/electrolyte interface (Q), additional capacitive contributions arising from pseudocapacitive behavior within the catalyst layer (Q_1), such as adsorption/desorption of reaction intermediates (e.g., *OH, *O, *OOH in OER), or ion transport capacitance in porous structures.

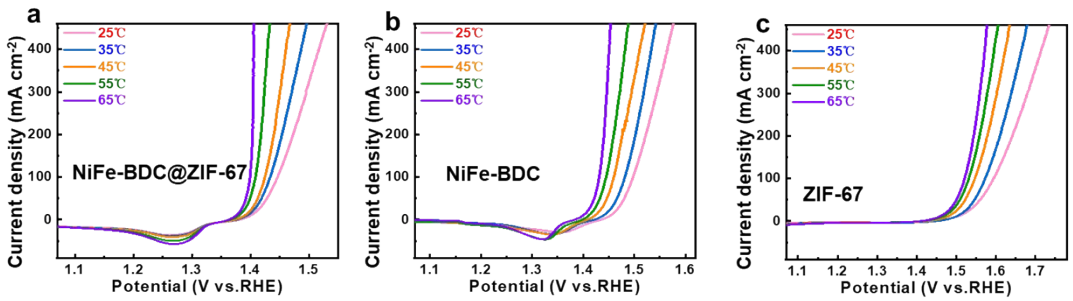

Figure S8 LSV curves of different samples in 1 M KOH electrolyte at different temperature.

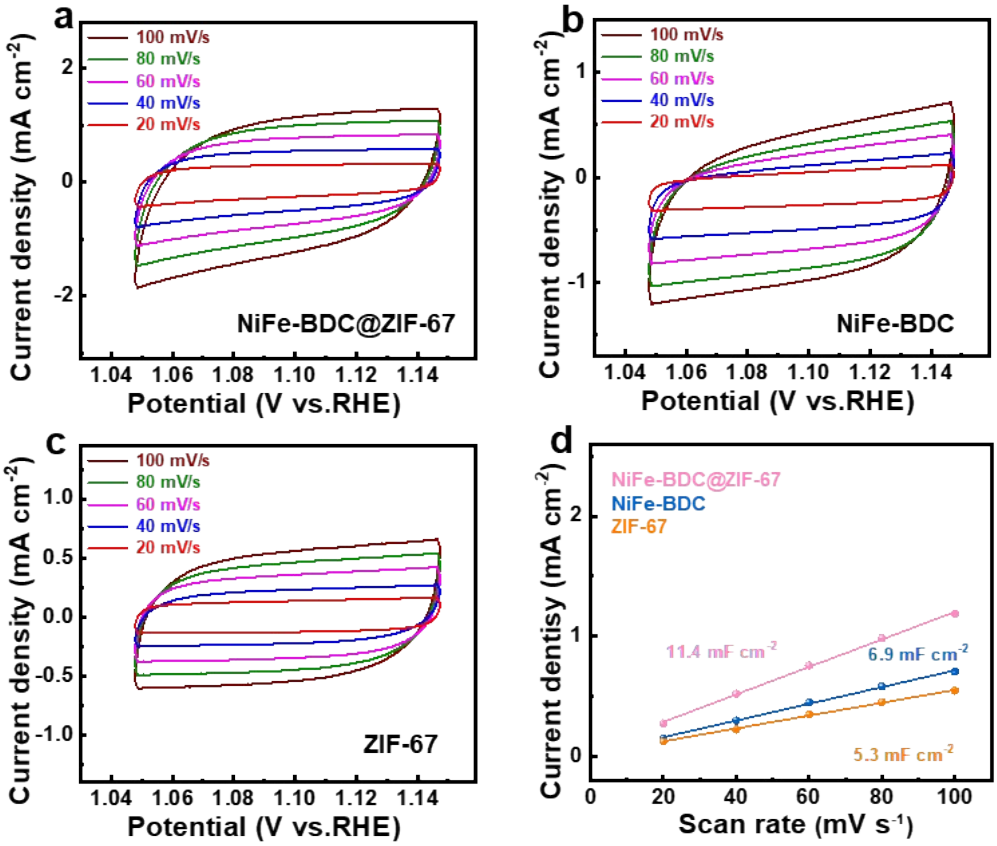

Figure S9 CV curves of the (a) NiFe-BDC@ZIF-67, (b) NiFe-BDC and (c) ZIF-67 at different scan rates in 1 M KOH solution. (d) The C_{dl} values of different samples.

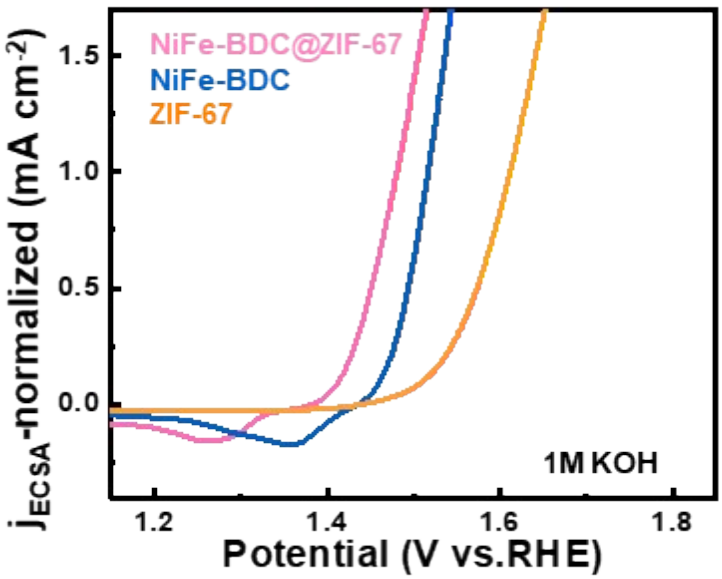

Figure S10 The normalized LSV polarization curve of different samples.

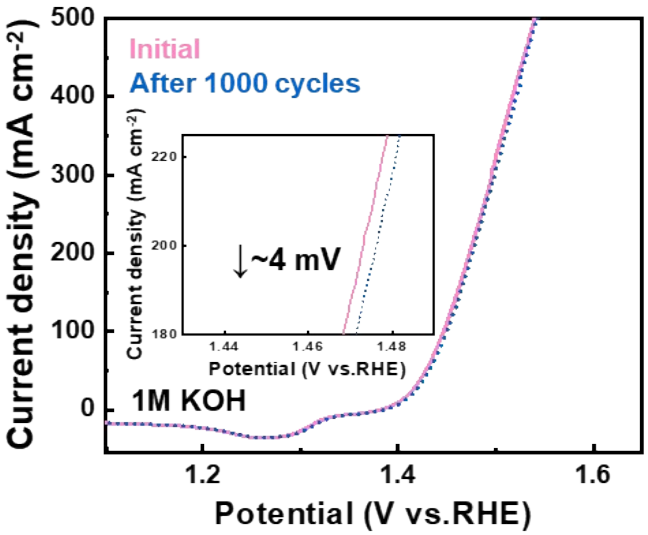

Figure S11 Polarization curves of NiFe-BDC@ZIF-67 at the initial and 1001st cycles.

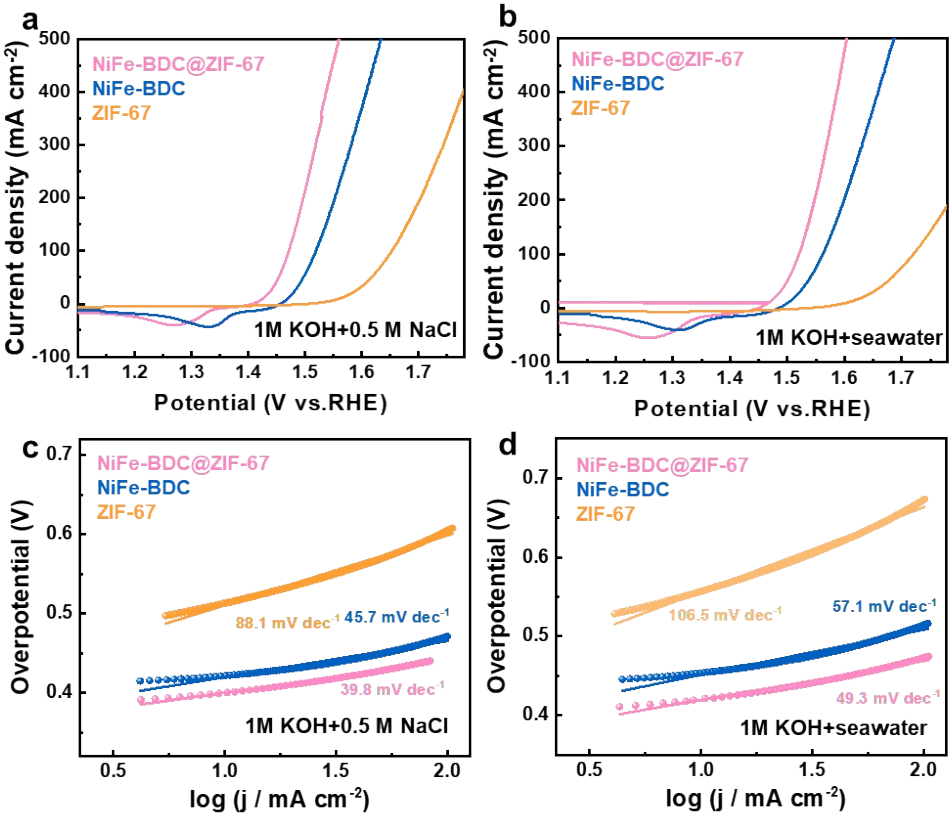

Figure S12 (a, b) LSVs, (c, d) Tafel slopes of different samples.

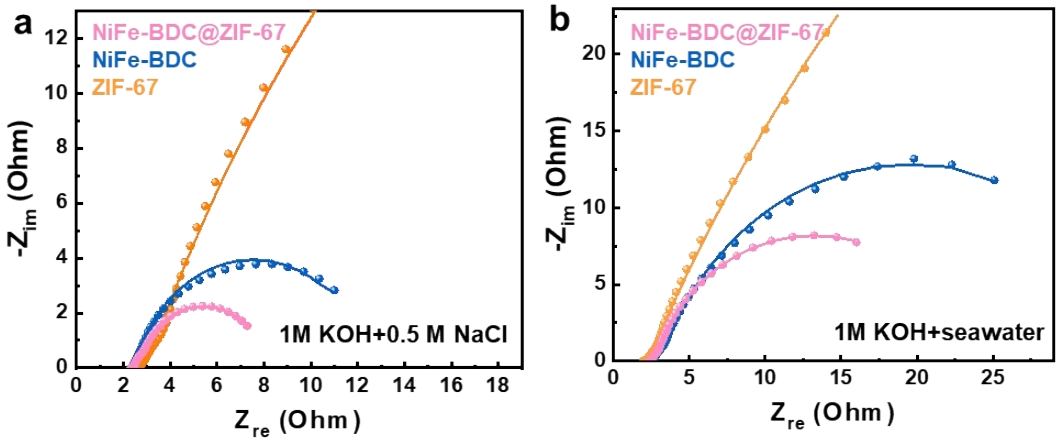

Figure S13 EIS of different samples.

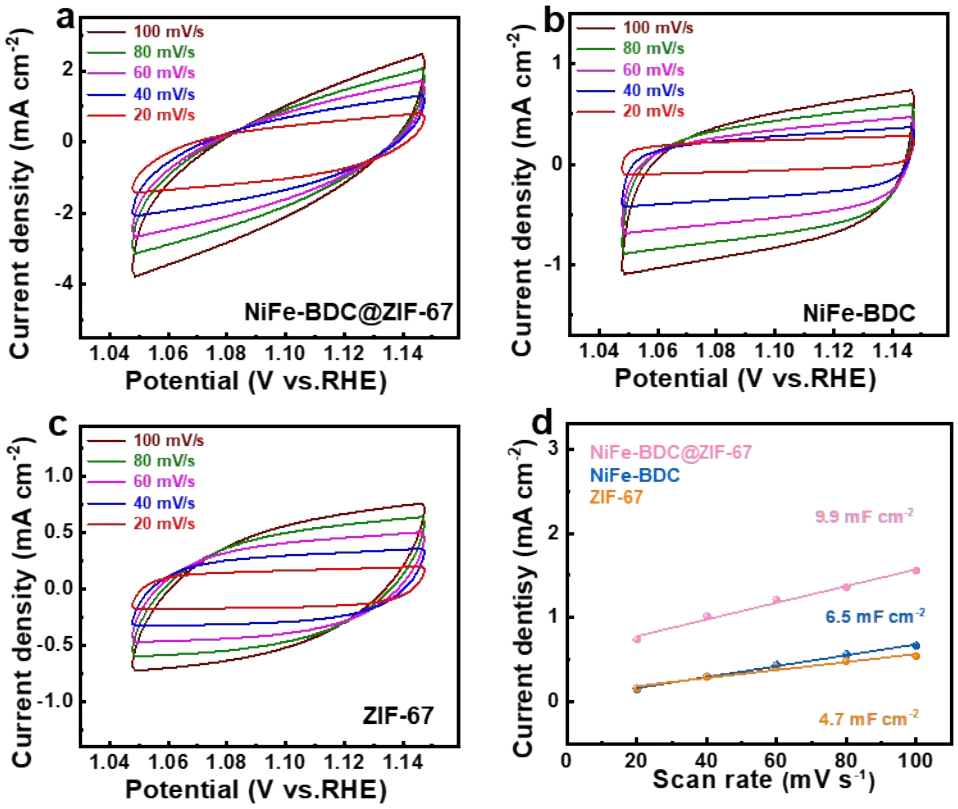

Figure S14 CV curves of the (a) NiFe-BDC@ZIF-67, (b) NiFe-BDC and (c) ZIF-67 at different scan rates in 1 M KOH + 0.5 M NaCl solution. (d) The C_{dl} values of different samples.

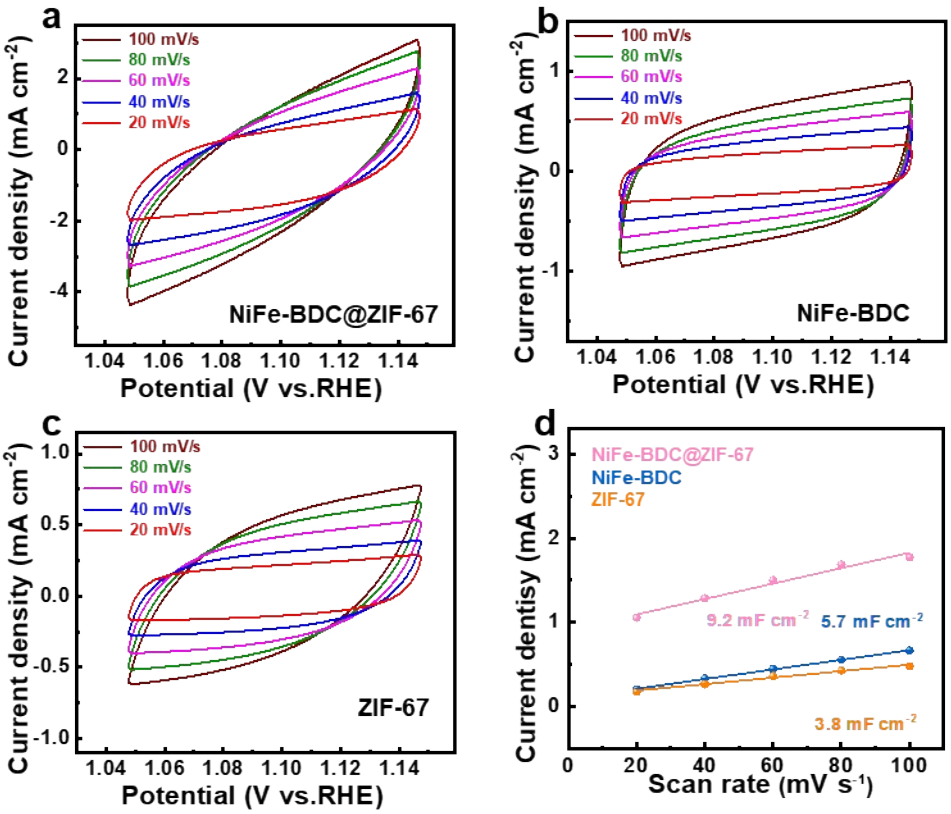

Figure S15 CV curves of the (a) NiFe-BDC@ZIF-67, (b) NiFe-BDC and (c) ZIF-67 at different scan rates in 1 M KOH + seawater solution. (d) The C_{dl} values of different samples.

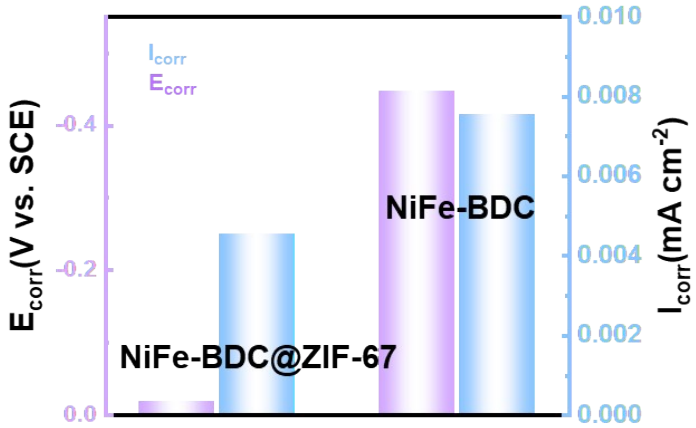

Figure S16 Comparison of corrosion current density (I_{corr}) and corrosion potentials (E_{corr}) in 1 M KOH + seawater solution.

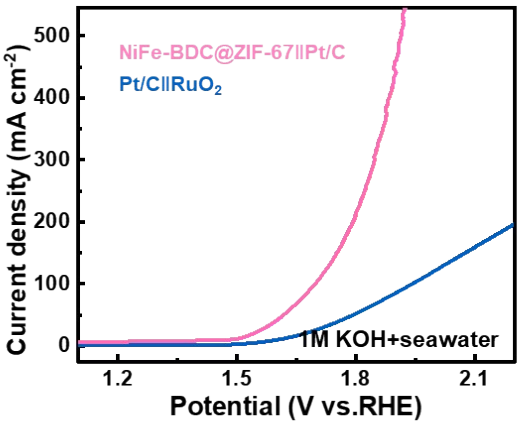

Figure S17 Overall seawater splitting of NiFe-BDC@ZIF-67 in 1 M KOH + seawater solution.

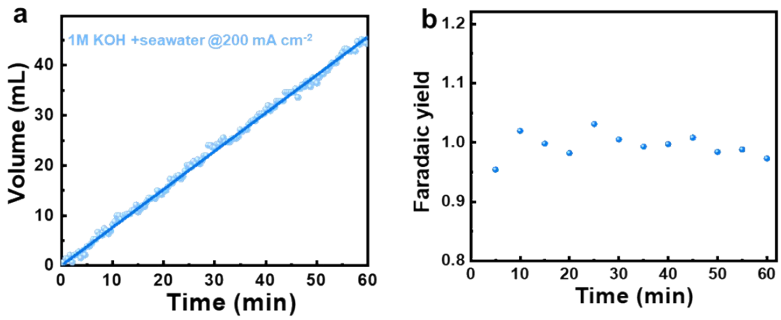

Figure S18 (a) Faraday efficiency of NiFe-BDC@ZIF-67 in 1 M KOH + seawater electrolyte. (b) The calculated result derived from the different time points in (a).

$$Faradaic\ yield\ (5min) = \frac{V_{Exp}}{V_{Theor}} = \frac{3.63416}{3.80857} \approx 0.954$$

According to the pressure-tracking method, the yields at subsequent time points are listed as follows: 10 min, 101.9%; 15 min, 99.8%; 20 min, 98.2%; 25 min, 103.1%; 30 min, 100.5%; 35 min, 99.3%; 40 min, 99.7%; 45 min, 100.8%; 50 min, 98.4%; 55 min, 98.8%; and 60 min, 97.3%. Starting from the 15th minute, the Faradaic efficiency stabilizes within a range of 97.3% to 103.1%, with an average value of 99.9% (standard deviation of 1.8%). These data clearly confirm that the experimental oxygen production measured by the pressure method is in good agreement with the theoretical values.

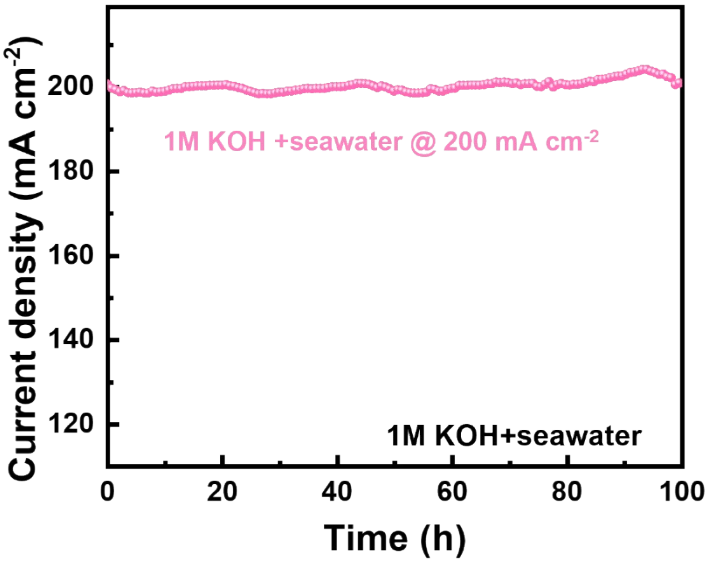

Figure S19 Long-term stability test in 1 M KOH + seawater solution.

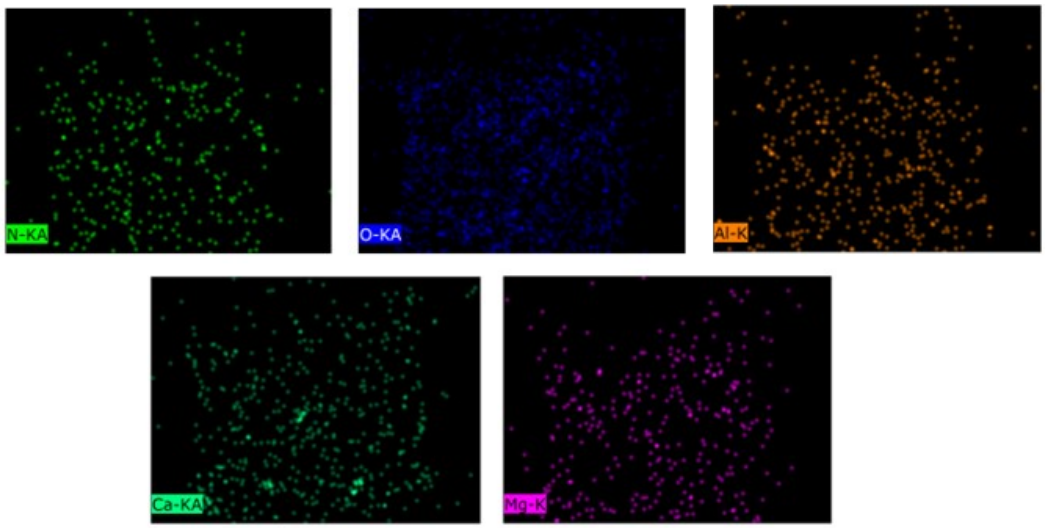

Figure S20 Elemental mapping of NiFe-BDC@ZIF-67 after OER test in 1 M KOH + seawater solution.

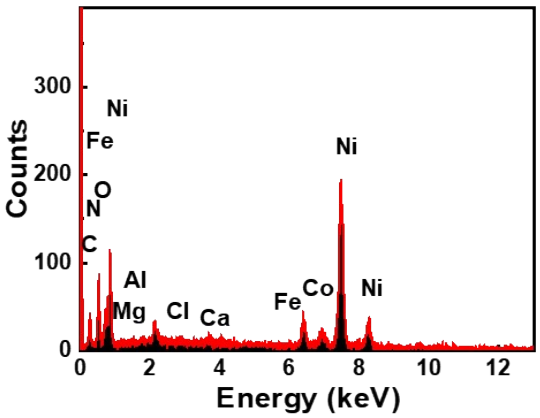

Figure S21 EDS pattern of NiFe-BDC@ZIF-67 after OER test in 1 M KOH + seawater solution.

Table S1. The impedance fitting parameters of different catalysts in 1 M KOH solution.

Catalysts	R_s/Ω	R_{ct}/Ω	R_1/Ω	χ^2
NiFe-BDC@ZIF-67	2.62	5.44	0.24	1.44×10^{-4}
NiFe-BDC	2.76	8.11	0.89	1.78×10^{-4}
ZIF-67	2.78	42.25	0.64	1.62×10^{-4}

Table S2. The values of C_{dl} and ECSA of of different catalysts in 1 M KOH.

Catalysts	C_{dl} (mF cm^{-2})	ECSA (cm^2)
NiFe-BDC@ZIF-67	11.4	285
NiFe-BDC	6.9	172.5
ZIF-67	5.3	132.5

Table S3. Comparison of the present work with recently reported OER catalysts.

Catalysts	Electrolyte	Overpotential (mV)	Ref
NiFe-BDC@ZIF-67	1 M KOH	η_{100}=217	**This work**
	1 M KOH + 0.5 M NaCl	η_{100}=241	
	1 M KOH + seawater	η_{100}=290	
Ni NDC@Fe BDC/CP	1 M KOH	η_{100}=239	1
NH_2-MIL-88B@ZIF-67	1 M KOH	H_{50}=302	2
MOF-(74 + 274)@NFF	1 M KOH	η_{50}=228	3
Ni-BDC/NM88B(Fe)	1 M KOH	η_{100}=232	4
	1 M KOH + 0.5 M NaCl	η_{100}=244	
	1 M KOH + seawater	η_{100}=299	
NiFe-BDC	1 M KOH	η_{100}=234	5
	1 M KOH + 0.5 M NaCl	η_{10}=220	
	1 M KOH + seawater	η_{10}=250	
Ni-Co-MOF-150	1 M KOH	η_{20}=320	6
	1 M KOH + 0.5 M NaCl	η_{50}=370	
PBA/NF-2h	1 M KOH	η_{100}=311	7
	1 M KOH + seawater	η_{50}=320	
$Ni(OH)_2$/NiFe-PBA	1 M KOH	η_{10}=247	8
	1 M KOH + 0.5 M NaCl	η_{10}=249	
	1 M KOH + seawater	η_{10}=292	
FNMO/NF	1 M KOH	η_{100}=251	9
	1 M KOH + 0.5 M NaCl	η_{100}=257	
	1 M KOH + seawater	η_{100}=269	
FeMn-MOF	1 M KOH	η_{100}=248	10
	1 M KOH + 0.5 M NaCl	η_{100}=255	
NiFe-LDH/MOF	1 M KOH	η_{100}=275	11
	1 M KOH + seawater	η_{100}=307	
Ni_3Fe-TPA/NF	1 M NaOH + seawater	η_{100}=301	12

Table S4. Comparison of the present work with recently reported OER catalysts.

Catalysts	Electrolyte	CA (h)	Ref
NiFe-BDC@ZIF-67	1 M KOH + 0.5 M NaCl	200 mA cm^{-2}, 100h	This work
	1 M KOH + seawater	200/500 mA cm^{-2}, 100h	
Ni-BDC/NM88B(Fe)	1 M KOH + 0.5 M NaCl	330 mA cm^{-2}, 28h	4
	1 M KOH + seawater	360 mA cm^{-2}, 28h	
Ni-Co-MOF-150	1 M KOH + 2.5 M NaCl	50 mA cm^{-2}, 20h	6
	1 M KOH + 3.5 M NaCl		
PBA/NF-2h	1 M KOH + seawater	50 mA cm^{-2}, 50h	7
FNMO/NF	1 M KOH + seawater	100 mA cm^{-2}, 2.22h	9
FeMn-MOF	1 M KOH + 0.5 M NaCl	100 mA cm^{-2}, 100h	10
NiFe-LDH/MOF	1 M KOH + seawater	20 mA cm^{-2}, 100h	11
Ni_3Fe-TPA/NF	1 M NaOH + seawater	10 mA cm^{-2}, 24h	12
CQD@NiFe-TDC-0.03	1 M KOH + seawater	100 mA cm^{-2}, 100h	13
aHE-MOF	1 M KOH + seawater	10 mA cm^{-2}, 100h	14
NFBF(6:2)	1 M KOH + 0.5 M NaCl	50 mA cm^{-2}, 24h	15
	1 M KOH + seawater		

Table S5. The impedance fitting parameters of different catalysts in 1 M KOH + 0.5M NaCl.

Catalysts	R_s/Ω	R_{ct}/Ω	R_1/Ω	χ^2
NiFe-BDC@ZIF-67	2.35	5.82	0.18	1.79×10^{-4}
NiFe-BDC	1.57	9.31	0.79	5.28×10^{-4}
ZIF-67	2.33	98.76	1.07	4.24×10^{-4}

Table S6. The impedance fitting parameters of different catalysts in 1 M KOH + seawater.

Catalysts	R_s/Ω	R_{ct}/Ω	R_1/Ω	χ^2
NiFe-BDC@ZIF-67	2.39	21.39	0.63	2.04×10^{-4}
NiFe-BDC	2.55	31.54	1.05	3.94×10^{-4}
ZIF-67	1.91	217.4	0.46	5.31×10^{-4}

Table S7. The values of C_{dl} and ECSA of different catalysts in 1 M KOH + 0.5M NaCl.

Catalysts	C_{dl} (mF cm^{-2})	ECSA (cm^2)
NiFe-BDC@ZIF-67	9.9	247.5
NiFe-BDC	6.5	162.5
ZIF-67	4.7	117.5

Table S8. The values of C_{dl} and ECSA of different catalysts in 1 M KOH + seawater.

Catalysts	C_{dl} (mF cm^{-2})	ECSA (cm^2)
NiFe-BDC@ZIF-67	9.2	230
NiFe-BDC	5.7	142.5
ZIF-67	3.8	95

Table S9. Comparison of the present work with recently reported overall splitting catalysts.

Catalysts	Electrolyte	Overpotential (V)	Ref
Pt/C‖NiFe-BDC@ZIF-67	1 M KOH + seawater	η_{10}=1.48, η_{200}=1.79, η_{500}=1.91	This work
PBA/NF-2h‖PBA/NF-2h	1 M KOH + seawater	η_{100}=1.83	7
Pt/C/NF‖FNMO/NF	1 M KOH + seawater	η_{100}=1.66	9
Pt/C‖NiFe-LDH/MOF	1 M KOH + seawater	η_{10}=1.524	11
Pt/C‖Ni_3Fe-TPA/NF	1 M KOH + seawater	η_{10}=1.56	12
NFBF(6:2)‖NFBF(6:2)	1 M KOH + seawater	η_{10}=1.44, η_{100}=1.80	15
Ir@NiFe-MOF/NF‖Ir@NiFe-MOF/NF	1 M KOH + seawater	η_{10}=1.49, η_{100}=1.84, η_{100}=2.43	16
Pt/C‖Fe-CoCo-PBA	1 M KOH + seawater	η_{10}=1.53	17
RhCoNi-MOF‖RhCoNi-MOF	1 M KOH + seawater	η_{10}=1.52, η_{100}=1.95	18
NiCo-aMOF3‖Ni-aMOF	1 M KOH + seawater	η_{10}=1.40, η_{340}=2.3	19
CdFe-BDC‖CdFe-BDC	1 M KOH + seawater	η_{10}=1.68	20

References

1. H. Yin, M. Huang, L. Wang, S. Muhammad, T. T. Isimjan, J. Guo, D. Cai, B. Wang and X. Yang, *Appl. Catal. B-Environ and Energy.*, 2025, **367**, 125105.

2. L. Ou, L. Xu, J. Guo, X. Yuan, Y. Jin, Q. Wang and X. Xiong, *J. Alloys Compd.*, 2025, **1017**, 179011.
3. Y. Jiang, T.-Y. Chen, J.-L. Chen, Y. Liu, X. Yuan, J. Yan, Q. Sun, Z. Xu, D. Zhang, X. Wang, C. Meng, X. Guo, L. Ren, L. Liu and R. Y.-Y. Lin, *Adv. Mater.*, 2024, **36**, 2306910.
4. Y. Bao, H. Ru, Y. Wang, K. Zhang, R. Yu, Q. Wu, A. Yu, D.-S. Li, C. Sun, W. Li and J. Tu, *Adv. Funct. Mater.*, 2024, **34**, 2314611.
5. G. Na, H. Zheng, M. Chen, H. Sun, T. Zhou, Y. Wu, D. Li, Q. Lu, Y. Chen, J. Zhao, Y. Zhang, T. He, B. Xiao, J. Zhang, F. Liu, H. Cui and Q. Liu, *J. Colloid Interf. Sci.*, 2025, **678**, 795-805.
6. P. Thangasamy, T.-G. Vo, R. Venkatramanan, Y.-T. Ng, J. Gao and Y. Liu, *Inorg. Chem.*, 2025, **64**, 5586-5597.
7. Y. Wang, D. Jia, W. Zhang, G. Jia, H. Xie, W. Ye, G. Zhu and P. Gao, *Chem. Commun. (Cambridge, U. K.)*, 2022, **58**, 6132-6135.
8. W. Shi, Y. Song, Q. Li, J. He, Z. Zhang, X. Zhang, X. Zhang and L. Zhang, *Chem. Commun. (Cambridge, U. K.)*, 2025, **61**, 12389-12392.
9. J.-Y. Gao, Y.-L. Ma, G.-S. Qian, M.-Y. Si, L.-L. Han and J.-S. Li, *Chem. Commun. (Cambridge, U. K.)*, 2024, **60**, 14224-14227.
10. R. Yuan, C. Liao, L. Cao, D. Li, S. Sun, G. Wang, G. Li, J. Xie and Z. Shao, *Adv. Funct. Mater.*, 2025, **36**, e08413.
11. M. Xiao, C. Wu, J. Zhu, C. Zhang, Y. Li, J. Lyu, W. Zeng, H. Li, L. Chen and S. Mu, *Nano Res.*, 2023, **16**, 8945-8952.
12. L. Xiao, X. Bai, J. Han, T. Tang, S. Chen, H. Qi, C. Hou, F. Bai, Z. Wang and J. Guan, *Nano. Res.*, 2023, **17**, 2429-2437.
13. Y. Zhang, H. Zhou, P. Zhao, K. Yuan, R. Zhou, H. Gao, Y. Qu and Y. Wang, *Fuel*, 2025, **389**, 134609.
14. J.-Y. Zhang, X.-L. Chen, Q. Wang, X.-S. Liu, J.-S. Liu, F. Dai, Z.-J. Liu and N. Zhang, *ACS Appl. Mater. Interf.*, 2026, **18**, 1382-1392.
15. S. Fan, X. Han, L. Li, Y. Xu, W. Gao, Y. Zhang, Z. Gao and C. Wang, *Nano. Res.*, 2025, **18**, 94907305.
16. H. Wang, Z. Li, Z. Cai, C. Yang, S. Sun, X. Wang, M. Zhang, M. Yue, D. Zheng, A. Farouk, M. S. Hamdy, X. Sun and B. Tang, *J. Mater. Chem. A*, 2024, **12**, 31121-31126.
17. S. Li, Z. Hu, Y. Zheng, T. Jia, X. Li, Y. Wang, Q. Wu, X. Zhu, L. Su, N. Yu, Y. Zhou, J. Lu and H. Tao, *Chem. Eng. J.*, 2025, **526**, 171075.
18. N. Q. Tran, T. T. Truong, T. T. N. Tran, T.-K. Truong, J. Yu, T. D. Nguyen, T. A. Le, C. C. Nguyen, L. H. T. Nguyen, N. H. Vu, Y. Kawazoe, T. B. Phan and T. L. H. Doan, *ACS Sustain. Chem. Eng.*, 2024, **12**, 1038-1050.
19. V. Sharma, P. Gnanasekar, R. Ahmad, L. O. Alimi, K. M. Aguliar Perez, L. Cavallo, B. S. Ooi and N. M. Khashab, *Chem. Mater.*, 2024, **36**, 5678-5686.
20. Y. Luo, X. Yang, L. He, Y. Zheng, J. Pang, L. Wang, R. Jiang, J. Hou, X. Guo and L. Chen, *ACS Appl. Mater. Interf.*, 2022, **14**, 46374-46385.